



Influence of detailed ball-and-socket modelling on tilting pad journal bearings dynamics

Štěpán Dyk¹ · Jan Rendl¹ · Radek Bulín¹ ·
Luboš Smolík¹

Received: 11 November 2022 / Accepted: 15 January 2023 / Published online: 9 February 2023
© The Author(s) 2023

Abstract The paper focuses on local phenomena modelling in the ball-and-socket pivot of tilting pad journal bearings. It provides an in-depth analysis of the influence of nonlinear normal force and friction forces generated in the pivot on the dynamic behaviour of the bearing. Contemporary works often employ the Hertz theory, which is valid for non-conformal contacts. This research, however, utilises a conformal sphere-to-sphere contact and uses the Bengisu-Akay and LuGre models, which describe static and dynamic friction. Furthermore, the latter model respects effects such as presliding, which can be essential for accurate predictions of nonlinear behaviour and which has not been employed to simulate the dynamics of the tilting pad journal bearings so far. This work also discusses the influence of model parameters. Such a discussion is critical for the LuGre model, whose proper parameter values are not straightforward to estimate.

Keywords Tilting pad journal bearings · Ball-and-socket · Friction · Conformal contact · LuGre model · Bengisu-Akay model

List of symbols

J	Journal indication
s	Pad indication
bs	Ball-and-socket indication
i	i -th pad
hd	Hydrodynamic component
m_J	Journal mass
m_s	Pad mass
I_P	Moment of inertia of pad relative to pivot point
$y_J(t)$	Journal centre vertical displacement
$z_J(t)$	Journal centre horizontal displacement
$\delta(t)$	Tilting angle of pad
$\eta(t)$	Radial displacement of pad, ball-and-socket penetration
C_ξ	Centre of gravity in tangential direction relative to pivot point
C_η	Centre of gravity in radial direction relative to pivot point
$\Delta m E$	Static unbalance
ω	Rotor angular speed
g	Gravitational acceleration
F_{hd}	Hydrodynamic force
F_{bs}	Normal force in ball-and-socket coupling
F_f	Friction force

Š. Dyk · J. Rendl (✉) · R. Bulín · L. Smolík
Faculty of Applied Sciences, NTIS – New Technologies for
the Information Society Research Centre, University of
West Bohemia, Technická 8, Pilsen, Czech Republic
e-mail: rendlj@ntis.zcu.cz

Š. Dyk
e-mail: sdyk@ntis.zcu.cz

R. Bulín
e-mail: rbulin@ntis.zcu.cz

L. Smolík
e-mail: carlist@ntis.zcu.cz

M_f	Friction moment
t	Time
R_1, R_2	Ball and socket radius
ΔR	Radius difference, $\Delta R = R_2 - R_1$
E_1, E_2	Young's modulus of ball and socket
μ_1, μ_2	Poisson's ratio of ball and socket
f_s	Static friction coefficient
f_d	Dynamic friction coefficient
χ	Parameter of BA model
v_c	Critical velocity of BA model
v_s	Stribeck velocity of LuGre model
γ	Exponent γ of LuGre model
σ_0^A	Bristle stiffness of LuGre model
σ_1^A	Bristle damping of LuGre model
σ_2^A	Viscous damping of LuGre model
v	Surface velocity in ball-and-socket
z_b	State variable, average deformation of bristles
N_m	Order of the BS coupling load magnitude
R_J	Journal radius
R	Inner radius (bore) of pad
L	Axial length of pad
c_m	Machined radial clearance
c_r	Assembled radial clearance
d	Pad thickness
N	Number of pads
ϑ	Angular position of pivot point
κ	Radial distance from pivot point to inner surface of pad
θ_1	Angular distance from pivot point to leading edge
θ_2	Angular distance from pivot point to trailing edge
X	Circumferential coordinate for pressure calculation
Z	Axial coordinate for pressure calculation
μ_d	Fluid film dynamic viscosity

1 Introduction

Tilting pad journal bearings (TPJBs) contain movable pads that allow for geometry changes during the operation. The TPJBs are used for their high stability allowed by the bearing ability to adapt to various operating conditions. The tilting motion of the pad is mainly secured using flexible supports, *rocker pivots* or *spherical pivots* (so-called *ball-and-socket* (BS) construction). However, the pivot design can be challenging [1]

concerning wear on contact surfaces, material treatment of the contact surfaces or preventing failure due to the high load on the pivot.

Compared to the rocker pivots with a line contact, the BS pivots contain surface contact, implying under the equal load more significant friction. Due to the inherent friction in the BS pivots, the performance and self-adaptation of the TPJB can be lower compared to the TPJBs with other pivots. Works [2,3] compared the behaviour of two identical bearings experimentally – one with a rocker-backed pivot and one with a BS pivot. Whilst the rocker-backed bearing showed a straight-line journal centre locus, the bearing with the BS-pivoted pads had a curved path. From the viewpoint of linear rotordynamics, the cross-coupled stiffness terms were proved to be close to zero for the rocker-backed pads and nonzero for the BS pivots. The authors hypothesised that these phenomena are caused by friction in the BS pivots. Similar observations using an experimental rig with a five-pad TPJB were published in [4,5] with further focus on pad temperatures and power loss.

Some recent papers focus on friction modelling in the TPJBs. Based on the above-mentioned experimental results, Kim et al. [6] proposed a model that includes a static friction model in a BS pivot. They showed different behaviour of the TPJB under varying loads for bearing with and without friction. They also stated possible instability issues due to the presence of friction. He [7] analysed friction in a BS pivot thoroughly. He showed that the friction in the BS pivot could result in non-synchronous vibrations of the journal and pads. Finally, Kim et al. [8] focused on pivot friction from the viewpoint of nonlinear dynamics taking the following parameters as bifurcation ones: pivot radius, pad preload, pivot offset, and length-to-diameter ratio. They showed the influence of these parameters on stability and corresponding bifurcations. Lately, [9] provided a comprehensive nonlinear analysis of a five-pad TPJB concerning friction in a spherical pivot. The authors considered both the pitch and roll motions of the pads, and tested the influence of friction models (Stribeck vs Coulomb) on the response of the system. Shin and Palazzolo [10] compared TPJBs with cylindrical and spherical pivots considering a thermally bowed shaft and studied the so-called Morton effect, which is further described, e.g., in [11].

An important parameter that significantly influences the TPJB dynamics is pivot stiffness [12], which has

been investigated both experimentally [13] and computationally [14]. Concerning computational approaches, a widely used estimation of the pivot contact force or stiffness is based on the Hertz theory [14, 15]. However, this approximation is usually derived under the assumption of a non-conformal contact, which does not hold for the BS pivot, where the contact surface covers large areas on the contacting bodies. Hence, He [7] suggested and tested a model proposed in [16], which derives a semi-analytical nonlinear model of the pressure field in the contact BS surfaces based on the conformal contact assumption. However, there are also other approaches to deal with the BS pivot. A model proposed in [17] is based on a nonstationary mixed contact problem, whereas a model from [18] inherently include the adhesion effect.

The normal force in the BS pivot subsequently influences the friction moment acting on the pad during its tilting motion. Since friction is a highly complex phenomenon, many friction models and different approaches to its modelling have been introduced [19]. These models can be classified into two groups: so-called *static* and *dynamic* models. The static models are more straightforward and describe the friction force considering a force-velocity characteristic. On the other hand, the dynamic models have some additional degrees of freedom, so-called dynamic variables. These models were developed to describe some friction-related phenomena more realistically. For example, they describe the presliding effect, breakaway force, Stribeck effect, or stick–slip phenomenon. This paper uses one static and one dynamic model to demonstrate how friction influences the bearing performance. The Bengisu-Akay model [19, 20] represents the class of static models and the LuGre friction [19, 21] model represents the class of dynamic models.

Friction occurring in the BS pivot produces local forces, which are, however, critical for the global behaviour of the TPJB. This research presents the use of methods to evaluate the friction forces, which have yet to be employed in this particular application according to the literature survey shown above. In particular, a conformal contact theory is utilised to determine normal forces in the BS pivot, and the LuGre model describes resulting friction moments. The use of the LuGre model, which belongs to the class of dynamic friction models, allows for capturing of nonlinear phenomena such as stick–slip, breakaway force or presliding that have been neglected in the preceding research

articles. Moreover, the paper also proposes a simple model of a TPJB with BS pivots, which can be used to study the interaction between friction, hydrodynamic forces and the resulting dynamics. The model is suitable for the calibration of friction model parameters. Such calibration is critical because the LuGre model requires application-specific values for model parameters, and the values proposed in other research and employed in other applications can yield inaccurate results.

The rest of the paper is organised as follows. Section 2, presents the equations of motion for a TPJB (in Sect. 2.1), describes normal forces acting in conformal contacts (in Sect. 2.2) and introduces friction modelling using static and dynamic friction models (in Sect. 2.3). Section 3 proposes a benchmark model in the form of a four-pad TPJB in the load-between-pad configuration that includes hydrodynamic couplings and dry friction contacts. Section 4 deals with the numerical analysis of the proposed model and discusses the influence of friction parameters on the model behaviour. Finally, Sect. 5 gives some conclusions.

2 Mathematical model

This section introduces the TPJB mathematical model. In order to separate the fundamental effects of friction in the BS pivot from the performance of the whole rotor, the simplest Jeffcott-like rotor symmetrically supported by two identical TPJBs is considered. The general dynamical model is briefly discussed in Sect. 2.1 and following sections focus on pressure distribution in the BS pivot (Sect. 2.2) and on the description of friction in the pivot (Sect. 2.3).

2.1 Dynamic model of the tilting pad journal bearings

The mathematical model of the Jeffcott rotor of mass $2m_J$ assuming two lateral degrees of freedom (DoFs) y_J, z_J and supported by two TPJB each consisting of N pads is presented below. Each pad of the TPJB has two DoFs – tilting angle δ and radial displacement η . The radial displacement is assumed only in the case of the flexible BS coupling, and represents the deformation (penetration depth) of the pivot if it is positive. The authors developed the presented TPJB model originally in [22] assuming the BS coupling without friction. In this section, the model is briefly summarised for clarity.

The scheme of all applied forces is depicted in Fig. 1. All particular subsystems are subjected to gravity load due to gravitational acceleration g . Furthermore, the rotor operating at angular speed ω is loaded by harmonic excitation caused by static unbalance $\Delta m E$. The equations of motion (1) and (2) describe rotor displacements and (3) and (4) give the motion of the i -th:

$$m_J \ddot{y}_J = -m_J g + \Delta m E \omega^2 \cos(\omega t) + \sum_{i=1}^N F_{hd,i}^y \quad (1)$$

$$m_J \ddot{z}_J = \Delta m E \omega^2 \sin(\omega t) + \sum_{i=1}^N F_{hd,i}^z \quad (2)$$

$$I_{P,i} \ddot{\delta}_i + m_{s,i} C_{\xi,i} \ddot{\eta}_i = -F_{hd,i}^y (R + \kappa_i) - M_{f,i} - m_{s,i} g [C_{\xi,i} \sin(\vartheta_i - \delta_i) - C_{\eta,i} \cos(\vartheta_i - \delta_i)], \quad (3)$$

$$m_{s,i} \ddot{\eta}_i + m_{s,i} C_{\xi,i} \ddot{\delta}_i - m_{s,i} C_{\eta,i} \delta_i^2 = -F_{hd,i}^z - F_{bs,i} - m_{s,i} g \sin(\vartheta_i - \delta_i), \quad (4)$$

where $m_{s,i}$ is the i -th pad mass, $I_{P,i}$ is the moment of inertia related to pivot point P_i , the centre of gravity of is located at point $C_i = [C_{\xi,i}, C_{\eta,i}]$ in coordinate system $\xi_i \eta_i$ with origin in pivot P_i , R is the inner radius of the i -th pad, κ_i is the radial distance from the pivot to the inner surface, and ϑ_i is the angular coordinate describing the the location of the i -th pivot. For more details on geometry, see [22].

Mutual interaction between the journal and the i -th pad is described by hydrodynamic force components $F_{hd,i}^y, F_{hd,i}^z$ which are evaluated in the coordinate system fixed to the pad. The total hydrodynamic force acting on the journal is the sum of particular forces from each pad and the following transformation into the Cartesian coordinate system is used

$$\begin{bmatrix} F_{hd,i}^y \\ F_{hd,i}^z \end{bmatrix} = \begin{bmatrix} \cos(\vartheta_i - \delta_i) & \sin(\vartheta_i - \delta_i) \\ -\sin(\vartheta_i - \delta_i) & \cos(\vartheta_i - \delta_i) \end{bmatrix} \begin{bmatrix} F_{hd,i}^y \\ F_{hd,i}^z \end{bmatrix}. \quad (5)$$

The particular hydrodynamic forces acting on the journal are evaluated using the pressure field generated in the corresponding bearing gap as follows:

$$\begin{bmatrix} F_{hd,i}^y \\ F_{hd,i}^z \end{bmatrix} = - \int_{-\frac{L}{2}}^{\frac{L}{2}} \int_{-R\theta_{2,i}}^{R\theta_{1,i}} p_i(X_i, Z_i, t) \begin{bmatrix} \sin \frac{X_i}{R} \\ \cos \frac{X_i}{R} \end{bmatrix} dX_i dZ_i, \quad (6)$$

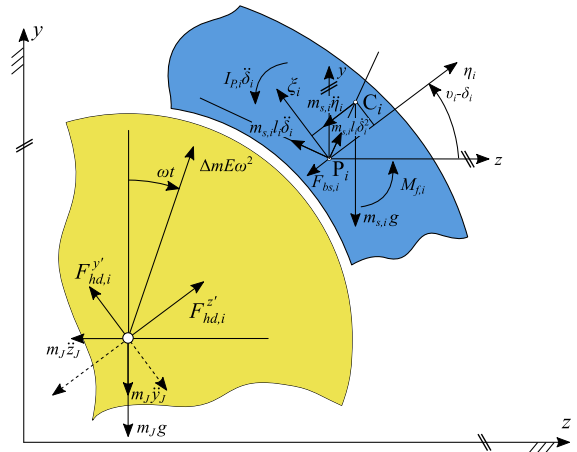


Fig. 1 Acting forces include gravitational forces $m_J g, m_{s,i} g$, out-of-balance force $\Delta m E \omega^2$, inertial forces ($m_J \ddot{y}_J, m_J \ddot{z}_J$ are acting on the journal and $I_{P,i} \ddot{\delta}_i, m_{s,i} \ddot{\eta}_i, m_{s,i} l_i \delta_i^2, m_{s,i} l_i \delta_i$ are acting on the i -th pad). The components of the hydrodynamic force $F_{hd,i}^y, F_{hd,i}^z$ acting on the journal are depicted by solid lines. The dashed lines depict the components of the hydrodynamic force acting on the pad. Normal force $F_{bs,i}$ denotes radial reaction in the BS coupling and moment $M_{f,i}$ is the friction moment

where p_i is the pressure field governed by the Reynolds equation, and X_i, Z_i are the circumferential and axial coordinates of the inner shell surface. The origin of coordinate system $X_i Y_i Z_i$ is fixed to the pad and lies on its inner surface. The radial distance between this origin and pivot point P_i is κ_i . Angles $\theta_{1,i}$ and $\theta_{2,i}$ denote the angular distance from the pivot point to the leading and trailing edges, respectively. For more details see the scheme depicted in [22]. The subroutines for necessary bearing gap formulation and coordinates transformation are shown in [22]. The boundary conditions for pressure field solution are prescribed at the edges as constants using relations

$$p_i(R\theta_{1,i}, Z_i, t) = p_{sup}, \quad (7)$$

$$p_i(-R\theta_{2,i}, Z_i, t) = p_{amb}, \quad (8)$$

$$p_i\left(X_i, -\frac{L}{2}, t\right) = p_{amb}, \quad (9)$$

$$p_i\left(X_i, \frac{L}{2}, t\right) = p_{amb}, \quad (10)$$

where p_{sup} and p_{amb} are supply and ambient pressures, respectively.

Next, each pad is loaded by normal radial force $F_{bs,i}$ as the reaction in the BS coupling and friction moment, which will be discussed in detail in the following sections.

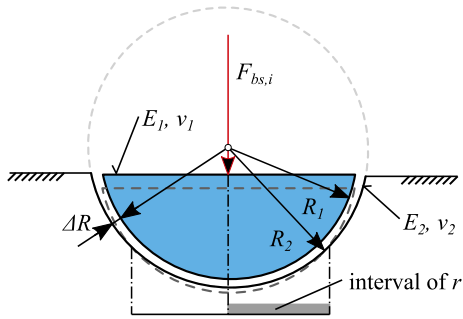


Fig. 2 Parameters of the BS conformal contact according to [16]

2.2 Normal forces in the BS coupling

As noted before, pressure distribution or normal force generated in the BS coupling are often modelled using the Hertz theory [14, 15, 23]. However, this theory usually assumes that the contact is non-conformal. In the case of the BS coupling, contact is not local compared to the dimensions of ball or socket bodies, and theories for conformal spherical surfaces are more suitable for the contact description. Further, we use a theory proposed by Fang et al. [16]. For the ball (subscript 1) and socket (subscript 2) coupling with Young’s moduli E_j , Poisson’s ratios μ_j , and with radii, R_j loaded by concentrated force $F_{bs,i}$, see Fig. 2, the employed theory leads to a set of nonlinear algebraic equations

$$p(r) = p_0 \left(1 - \frac{r^2}{a^2} \right)^n, \tag{11}$$

$$p_0 = (n + 1) \frac{F_{bs,i}}{\pi a^2}, \tag{12}$$

$$\eta = 4(k_1 + k_2) B p_0 a, \tag{13}$$

$$a = \left[\frac{4BR_1R_2(k_1 + k_2)F_{bs,i}}{\pi(g\Delta R + C)} \left(n + \frac{1}{2} \right) (n + 1) \right]^{1/3}, \tag{14}$$

$$n = \frac{1}{2} - 0.24e^{-15.08\left(1 - \frac{a}{R_2}\right)}, \tag{15}$$

$$B = \frac{\sqrt{\pi}\Gamma(n + 1)}{2\Gamma\left(\frac{3}{2} + n\right)}, \quad C = \frac{3.8304BF_{bs,i}(k_1 + k_2)}{\pi R_2}, \tag{16}$$

$$g(a) = \frac{2}{\pi} + \left(\frac{a}{R_2} \right)^2. \tag{17}$$

where p_0 is the maximum contact pressure, a is the projective radius of the contact area, r is the radius of the pressure field, n is the pressure distribution exponent.

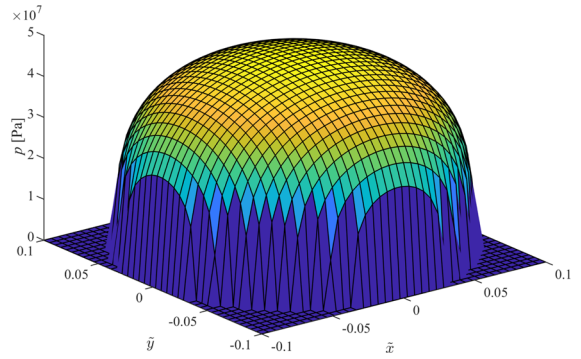


Fig. 3 Example of the pressure field in the BS coupling for radius difference $\Delta R = 0$. Coordinates \tilde{x} , \tilde{y} denote local coordinate system in the BS coupling

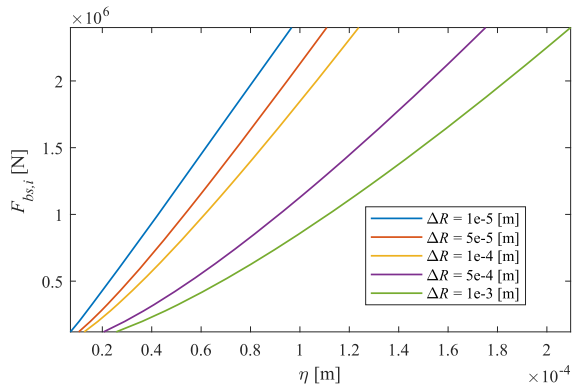


Fig. 4 Force $F_{bs,i}$ generated in the i -th BS coupling as a function of the penetration depth η_i for the chosen radius differences ΔR with conformal contact model [16]

Coefficients k_1, k_2 are defined as follows:

$$k_1 = \frac{1 - \mu_1^2}{\pi E_1}, \quad k_2 = \frac{1 - \mu_2^2}{\pi E_2}. \tag{18}$$

In equations (11) - (17), $\Gamma(n)$ stands for the gamma-function of n .

For illustration, the pressure field generated in the BS coupling is shown in Fig. 3. To demonstrate results of the used theory, let us assume contact of spherical surfaces with following parameters adopted from [16]: steel-on-steel contact ($E_1 = E_2 = 2.1 \cdot 10^{11}$ Pa, $\mu_1 = \mu_2 = 0.3$), radius of the socket $R_2 = 100$ mm, $R_1 = R_2 - \Delta R$ for various ΔR . The resulting force generated in the BS coupling for various radius differences is shown in Fig. 4.

In the subsequent numerical simulations, forces $F_{bs,i}$ are involved in the model as a function of pen-

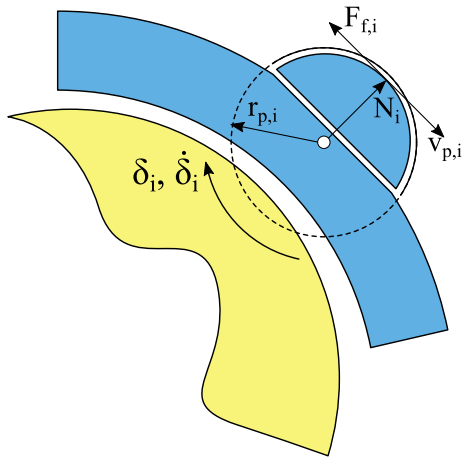


Fig. 5 The BS pivot of the TPJB

etration in the BS coupling

$$F_{bs,i} = F_{bs,i}(\eta_i). \tag{19}$$

Normal force at each time of integration step is evaluated based on look-up table. The look-up table consists of large precalculated values based on (11)–(17). Current value of penetration η yielding from numerical integration of equations of motion is then interpolated between two closest points from the table.

2.3 Friction in BS coupling

Subsequently, friction moments generated in the BS pivot were added to the model mentioned in Sect. 2. This additional friction moment acting to pad i can be generally written as (see Fig. 5)

$$M_{f,i} = R_{1,i} F_{f,i}(v_i), \tag{20}$$

where $r_{p,i}$ is ball radius and the particular form of friction force $F_{f,i}$ depends on the friction model used.

Velocity at the surface of the BS coupling is given in the form

$$v_i = R_{1,i} \dot{\delta}_i, \tag{21}$$

where $\dot{\delta}_i$ is the angular velocity of the pad tilting motion. The rolling motion was assumed not to happen¹.

First, the friction will be described using a static friction model. The Bengisu-Akay model [19,20] was

¹ The TPJB model considering both tilting and rolling motions is discussed in [9] in detail.

considered, which describes the force-velocity function as a piecewise smooth function that captures different values of static and dynamic friction coefficients

$$F_{f,i} = \begin{cases} -\frac{f_s F_{bs,i}}{v_c^2} (|v_i| - v_c)^2 + f_s F_{bs,i} \text{sign}(v_i) & \text{for } |v_i| < v_c \\ [f_d F_{bs,i} + (f_s F_{bs,i} - f_d F_{bs,i}) e^{-\chi(|v_i| - v_c)}] \text{sign}(v_i) & \text{for } |v_i| \geq v_c \end{cases} \tag{22}$$

where f_s, f_d are static and dynamic (kinetic) friction coefficients, v_c is the critical velocity that defines an area of friction force smooth transition around zero velocity, and χ expresses the shaping of the curve after reaching critical velocity.

To better describe such phenomena as presliding, stick–slip, breakaway forces, friction hysteresis or frictional lag, the LuGre friction model [21] will be used. Since the original LuGre model was developed for the constant normal force, the slightly modified form for the varying normal force introduced in [24–26] will be used. In this case, friction force generated in the pivot of i -th pad is given as²

$$F_{f,i} = \left(\sigma_0^A z_{b,i} + \sigma_1^A \dot{z}_{b,i} + \sigma_2^A v_i \right) F_{bs,i} \tag{23}$$

where σ_0^A represents the aggregate stiffness of the fictional bristles per unit of the normal force, σ_1^A is their corresponding aggregate damping, and σ_2^A is the parameter of viscous friction. An additional state variable $z_{b,i}$ (average deformation of fictional bristles in the contact surface) from equation (23) is described by the first-order ordinary differential equations

$$\dot{z}_{b,i} = v_i - z_{b,i} \frac{\sigma_0^A |v_i|}{G^A(v_i)}. \tag{24}$$

and function $G^A(v_i)$ is here given as

$$G^A(v_i) = f_d + (f_s - f_d) e^{-|v_i/v_s|^\gamma}, \tag{25}$$

where γ is a parameter that defines the shape of the Stribeck curve.

The main issue of the LuGre model is the proper setting of its parameters. It is advised to perform experimental identification of friction model parameters as it is described, e.g. in [27]. However, this kind of experiment cannot be performed for the complex mechanical system described in Sect. 2.1. In the presented case, the BS coupling is loaded by force, whose amplitude can reach tens of thousands of newtons. Thus,

² Superscript A stands for *amended* as denoted in [25].

Table 1 Parameters of the TPJB adopted from [28]

Parameter		Value	Unit
Journal radius	R_J	49.9	mm
Pad inner radius	R	50	mm
Pad axial length	L	100	mm
Machined radial (half) clearance	c_m	100	μm
Assembled radial (half) clearance	c_r	80	μm
Pad preload	–	0.2	–
Pad thickness	d	14	mm
Angular pad length	$\theta_1 + \theta_2$	69.3	deg
Pivot ratio	–	0.5	–
Pivot radial distance from inner shell	κ	14	mm
Journal mass	m_J	2000	kg
Pad mass	m_s	0.8108	kg
Pad moment of inertia	I_P	$4.055 \cdot 10^{-4}$	$\text{kg} \cdot \text{m}^2$
Pad centre of gravity	$[C_{\xi}, C_{\eta}]$	$[0, -10.1]$	mm
Fluid-film dynamic viscosity	μ_d	$19 \cdot 10^{-3}$	$\text{Pa} \cdot \text{s}$
Journal static unbalance	$\Delta m E$	$10 \cdot 10^{-3}$	$\text{kg} \cdot \text{m}$

the original LuGre friction model [21] which is suitable for constant normal contact forces is not appropriate and its modified form [24] is used. Since the LuGre model physical interpretation is based on the tangentially deforming bristles (asperities) of bodies in contact, which describes mainly the sticking phase of friction, it is appropriate to assume that with increasing normal contact force, the bristles' average stiffness also increases. This phenomenon is caused by higher mutual penetration of bristles and higher local deformation of the bodies, which increase the number of fictional bristles in contact. The study of suitable parameters for the LuGre friction model is further discussed in Sect. 3.1

3 Solution strategy and model parameters

The proposed model will be demonstrated considering the case of a four-pad TPJB with a load-between-pads (LBP) configuration. Its parameters adopted from [22, 28] are summarised in Table 1.

The simulations in the time domain are performed using Matlab built-in solver for stiff ordinary differential equations *ode15s* with relative error tolerance 10^{-6} and absolute error tolerance 10^{-8} . The initial positions are given as a solution of the static analysis (set of

nonlinear algebraic equations) and initial velocities are considered to be zero. The time interval of steady-state simulations is $t \in \langle 0; 2 \rangle$ s, which has been proved as long enough not to be influenced by initial conditions. In case of run-up simulations, longer time interval is considered $t \in \langle 0; 10 \rangle$ s.

The residual static unbalance applied on the rotor is calculated following standard ISO 21940-11 [29] as

$$\Delta m E = 9549 \frac{Gm}{n_{\max}} \left[\text{g} \cdot \text{mm} \right], \quad (26)$$

where the balance quality grade $G = 6.3 \text{ mm} \cdot \text{s}^{-1}$ was chosen for general machinery, m is the rotor mass, and n_{\max} is the maximum nominal rotor speed. In this work, $n_{\max} = 6500$ rpm was mainly investigated because various friction phenomena are fully developed at this nominal speed, and the value is near the original nominal speed in [28]. The system behaviour at lower rotor speeds and the effect of friction in the BS coupling are investigated using run-up simulations.

Parameters of the BS coupling are summarised in Table 2. A steel-on-steel contact in the BS is considered with the corresponding Young's moduli and Poisson's ratios. Three radius differences $\Delta R = R_{\text{socket}} - R_{\text{ball}}$ are taken into account in the range that corresponds to the machining precision. Both friction coefficients

Table 2 Parameters of the BS coupling and friction models

Parameter		Value	Unit
Socket radius	R_2	13	mm
Radius difference	ΔR	{0; 15; 30}	μm
Young's moduli	E_1, E_2	$2.1 \cdot 10^{11}$	Pa
Poisson's ratios	μ_1, μ_2	0.3	–
Static friction coefficient	f_s	{0; 0.2}	–
Dynamic friction coefficient	f_d	{0; 0.2}	–
Parameter of BA model	χ	1000	–
Critical velocity (BA)	v_c	10^{-5}	$\text{m}\cdot\text{s}^{-1}$
Stribeck velocity (LuGre)	v_s	10^{-3}	$\text{m}\cdot\text{s}^{-1}$
Exponent γ (LuGre)	γ	1	–
Bristle stiffness (LuGre)	σ_0^A	10^6	m^{-1}
Bristle damping (LuGre)	σ_1^A	10	$\text{s}\cdot\text{m}^{-1}$
Viscous damping (LuGre)	σ_2^A	0	$\text{s}\cdot\text{m}^{-1}$

f_s, f_d are taken from the interval $(0; 0.2)$ which is reasonable for the considered materials and conditions.

In all the forthcoming numerical analyses, we focus on the local behaviour in the BS coupling and the influence of the pivot friction on the TPJB performance. Hence, we minimise the influence of all other phenomena occurring in the TPJB, such as pad fluttering of the upper pads, pads' flexibility, etc. For this reason, only two lower pads are considered, and we neglect the influence of upper pads. As shown in [22], this simplification is justifiable since the upper pads do not have a load-carrying function during the chosen standard operation, and they are, under some conditions, even subjected to pad fluttering. Therefore, this phenomenon and the possible interaction of the pad fluttering with pivot friction is out of the scope of this paper. Lower pads only imply non-negative normal forces (19).

The choice of frictional parameters is discussed in Sect. 3.1 and their influence is a subject of the proposed study.

3.1 Discussion on suitable parameters of the friction models

Both studied friction models use similarly described Stribeck curves. In general, the Bengisu-Akay model parameter χ is the reciprocal value of the LuGre model parameter v_s . Then, for $\gamma = 1$, which is our setting, the resulting Stribeck curve is equal for both studied

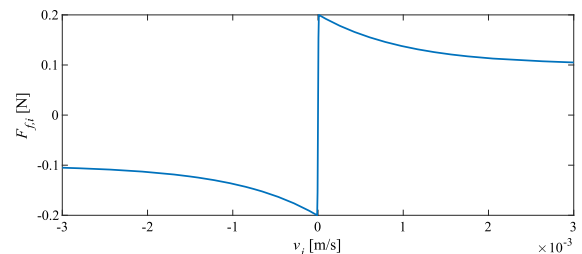


Fig. 6 Stribeck curve used in the simulations for $f_s = 0.2$, $f_d = 0.1$, $v_c = 10^{-5} \text{ m}\cdot\text{s}^{-1}$, $F_{bs,i} = 1 \text{ N}$, $\gamma = 1$ and $\chi = 10^3$ (Bengisu-Akay model)

models, so the results are comparable. For illustration, used friction characteristic for $f_s = 0.2$, $f_d = 0.1$, is shown in Fig. 6.

The usual value of the critical velocity v_c for the Bengisu-Akay model in multibody system dynamic problems is $0.001 \text{ m}\cdot\text{s}^{-1}$ [19]. This parameter defines an area around zero slip velocity, where the friction force is smoothed to prevent discontinuity. The smooth friction transition between positive and negative sliding velocities is needed because of the stability of the numerical solution. In the problem of the highly loaded BS coupling, the sliding velocities are relatively small, and a micro-sliding can occur. Thus it is necessary to set parameter v_c sufficiently low. Based on the problem analysis, it was found that the usual value is still too high to properly catch the friction force generated around the zero BS relative velocities. Thus, this

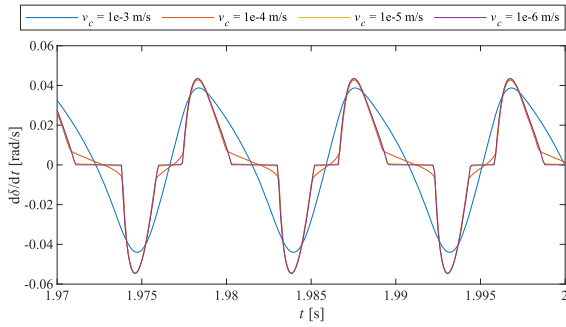


Fig. 7 Influence of critical velocity v_c on pad tilting velocity assuming rotor speed 6500 rpm and friction coefficients $f_s = 0.1$ and $f_d = 0.05$

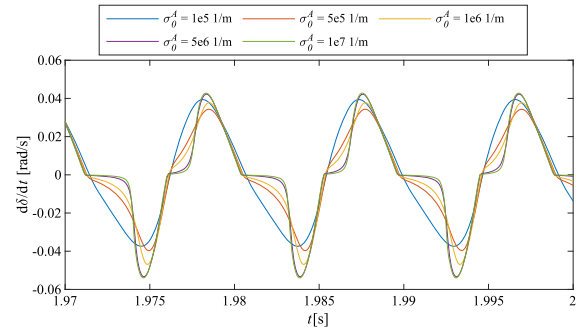


Fig. 8 Influence of bristle stiffness parameter σ_0^A on pad tilting velocity assuming rotor speed 6500 rpm and friction coefficients $f_s = 0.1$ and $f_d = 0.05$

parameter is set to $v_c = 10^{-5} \text{ m}\cdot\text{s}^{-1}$, which is closer to a non-smooth Coulomb model. A significant change in the pad tilting motion is documented in Fig. 7. For $v_c = 0.001 \text{ m}\cdot\text{s}^{-1}$ only sliding friction occurs, while with lower values the friction sticking is more apparent.

The bristle average stiffness from equation (23) can be expressed as $\sigma_0^A F_{bs,i}$ so it is apparent that it depends on the normal contact force and the physical unit of parameter σ_0^A is m^{-1} . In many works related to friction modelling, such as [19, 21], the bristle stiffness is considered as $10^5 \text{ N}\cdot\text{m}^{-1}$. This value can be valid only for lightly loaded contacts, as it is described in [30]. Unfortunately, there are not many references for the LuGre friction model behaviour in case of very high loads, but e.g. in [31], the LuGre model was verified to be suitable for modelling tire friction. The tire was loaded by 4 kN, and the resulting LuGre parameter was $\sigma_0^A = 3.117 \cdot 10^5 \text{ m}^{-1}$. In the problem of the highly loaded BS coupling, it is expected that sticking will not be as flexible as in the case of rubber tires. Thus its bristle stiffness-related parameter σ_0^A should be at least 10^6 m^{-1} or higher. Nevertheless, as it is stated in [32], with a further increase of σ_0^A the results do not differ significantly and only the required CPU time increases. The significant influence of the bristle stiffness parameter σ_0^A on the pad tilting motion is shown in Fig. 8. For lower σ_0^A almost no sticking occurs, while with higher σ_0^A the sticking phenomena together with presliding behaviour appear.

The LuGre parameter σ_1^A is related to the bristle damping in the presliding state, and its physical unit is $\text{s}\cdot\text{m}^{-1}$. In the case of the amended model, where both bristle stiffness and damping depend on the normal contact force, the value of the parameter σ_1^A needs

to be scaled accordingly to the normal contact force amplitude. In case of constant normal contact force, the commonly used values of the parameters of the Amended LuGre model satisfy the following equation

$$\sigma_1^A \cdot N_m = \sqrt{\sigma_0^A \cdot N_m}, \tag{27}$$

where N_m is the characteristic value of the normal contact force. Equation (27) comes from the standard setting of the parameters for the original LuGre model, where the value of bristle damping is set as the square root of bristle stiffness value [19]. It should also be mentioned that (27) is used only for obtaining the value of the parameters; only numerical values of each parameter are taken into account. As mentioned earlier, the order of magnitude of the BS coupling load is in tens of thousands of newtons. Thus, the corresponding value of σ_1^A can be set as

$$\sigma_1^A = \sqrt{\frac{\sigma_0^A}{N_m}}, \tag{28}$$

where the characteristic value of the normal contact force $N_m = 10^4 \text{ N}$ represents the order of magnitude of the BS coupling load, which appears in the model of presented system. With this setting, the overall bristle damping corresponds to common values used in the original LuGre model, while its normal contact force dependency is maintained. In our case, for $\sigma_0^A = 10^6 \text{ m}^{-1}$ the resulting bristle damping parameter, which comes from (28), is $\sigma_1^A = 10 \text{ s}\cdot\text{m}^{-1}$.

Based on the presented parametric study, the used values of friction parameters that can catch various friction phenomena are summarised in Tab. 2.

4 Simulation results and discussion

In this section, we show the results of the performed numerical analyses. First, Sect. 4.1 deals with the influence of the pad radial displacement due to the BS coupling deformation on the TPJB performance. Further, Sect. 4.2 discusses the influence of radius difference and Sect. 4.3 provides a detailed friction analysis. Finally, Sect. 4.4 shows transient simulations the run-up to demonstrate the differences in the journal trajectory due to friction.

Above all, let us mention that the influence of friction on the TPJB steady-state behaviour is given by the operation regime. The unbalance is estimated using (26) for the particular value of nominal rotor speed n_{\max} . For lower speeds, small unbalance forces generate a small journal orbit and a small tilting motion of the pad. Hence, the pads remain in the sticking regime. Similarly, the lower unbalance causes a stick in the BS coupling concerning the given nominal rotor speed. Therefore we demonstrate all the forthcoming steady-state simulations for nominal speed and corresponding unbalance, which induces the tilting motion in both stick and slip regimes.

4.1 Influence of pad radial displacement on the bearing performance

Performed analyses show the key influence of the pad radial displacement on the bearing performance. Simply speaking, the pad radial motion due to the elastic deformation of the BS coupling enlarges the bearing operational clearance, yielding a larger journal orbit. At the same time, the operating point of the journal moves downwards. This operation state then imposes a more significant tilting motion of the pads that emphasises the influence of friction phenomena.

To demonstrate the above-stated, we use two topologically different models:

Tilting-only (TO) model is a simplified model with the neglected radial displacement of the pads. In this case, the motion of pads is described by (3) only, and (4) is not taken into account.

Tilting-radial (TR) model includes both tilting and radial degrees of freedom described by (3) and (4).

Let us focus first on the frictionless cases. As shown in Fig. 9, the TO model yields smaller journal orbits

than the TR model. At the same time, the orbits are located higher compared to the TR model. This behaviour is caused due to the omission of the pivot deformation in the TO model.

Figure 9 shows that friction negatively influences the TPJB performance since the journal orbit gets larger in both cases. Here, we used Bengisu-Akay (BA) model with $f = f_s = f_d = 0.1$. The influence of friction will be discussed in detail in Sect. 4.3, but for now, we can state that the larger influence of friction occurs in the TR case, which is also more precise in the description of local phenomena in the BS coupling. Hence, we further focus on the TR-type model only.

4.2 Influence of the radius difference in the BS coupling

Previous analyses in Sect. 4.1 showed that the considered flexibility of the BS coupling has several impacts on the TPJB dynamics and has to be taken into account to predict the TPJB behaviour accurately. The BS coupling flexibility is controlled by the Fang nonlinear contact force model presented in Sect. 2.2 and strongly depends on the differential radius and penetration depth, see Fig. 4. Resulting force in the BS coupling $F_{bs,i}$ and applied concentrated normal force satisfy the force equilibrium. First, the friction is not assumed in the following simulations to separately study the influence of a radius difference of the BS coupling on the TPJB dynamics. Next, the friction influence is studied together with various radius differences.

The radius difference is varied considering $\Delta R = \{0, 15, 30\} \mu\text{m}$. Chosen values correspond to some typical clearance fits per ISO 286–1 [33]. $\Delta R = 0 \mu\text{m}$ is a limit case of the snug fit (e.g., H7/h6), allowing for a free assembly or disassembly. $\Delta R = 15 \mu\text{m}$ corresponds to the sliding fit (e.g., H7/g6), which allows for free turning and, finally, $\Delta R = 30 \mu\text{m}$ is the close running fit (e.g., H8/f7) used on accurate machines and up to moderate angular speeds. It is supposed that the snug fit, i.e. the case when the ball and socket have equal radius, is the stiffest option. The results are depicted and compared in the form of journal orbit and waveforms of tilting angle and velocity of the first pad in Fig. 10. The tilting-only model (TO) is assumed as a reference.

The attached subfigures clearly show that the journal moves downwards significantly with the increas-

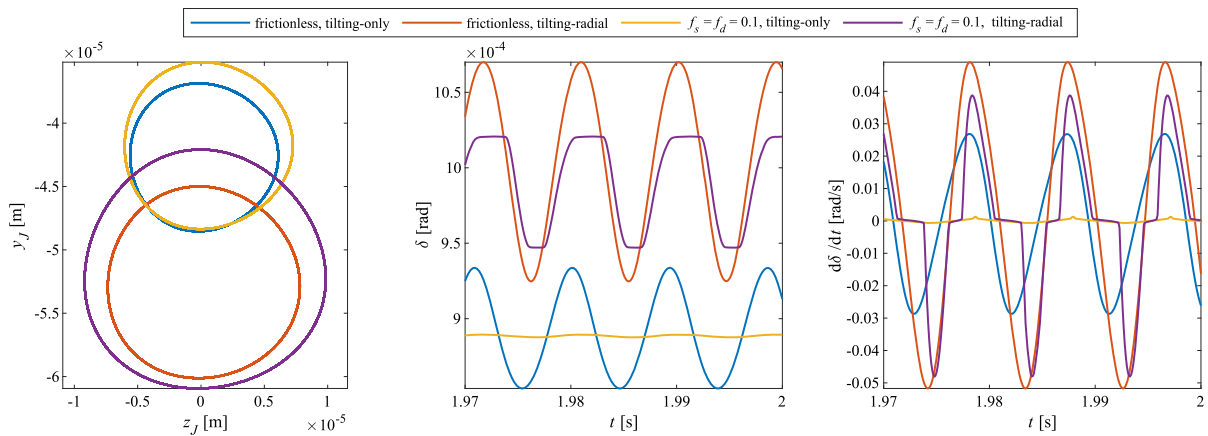


Fig. 9 Influence of the considered degrees of freedom of the pads on the journal orbit (left), the tilting angle of pad (centre) and its tilting velocity (right). All the results are depicted for a frictionless (FL) case and a case with friction (here, the Bengisu-

Akay model with $f = f_s = f_d = 0.1$ is used as an example), and for two considered cases: tilting-only (TO) and tilting-radial (TR) model of pads

ing radius difference, which causes the BS coupling to become more flexible. It should be noted that the downward movement is caused only by the contact stiffness, because the assembled clearance of the TPJB is equal in all analysed cases. Figure 10 also shows that the higher radius difference increases the tilting angle and tilting velocity. These changes demonstrate that the journal moves around a new equilibrium position, which means that the hydrodynamic force acting on each pad is also affected. We assume that the Fang model is more suitable for reaction force description in this situation due to its direct evaluation from penetration depth (degree of freedom) contrary to the necessary linearisation at each time step of numerical simulation and stiffness estimation based on the Hertz model.

The peak-to-peak amplitudes of the tilting angle and velocity displacement increase with the radius difference, although the bearing assembled clearance remains the same. This observation confirms that the radius difference decreases the dynamic stiffness of the pivot, which acts as an additional artificial bearing clearance. Therefore, the journal can perform larger orbital motions when the radius difference increases. Such behaviour occurs for both TO and TR models. When friction is applied using the Bengisu-Akay model, the waveforms flatten due to the sticking phenomenon occurring at low pad velocities.

4.3 Influence of friction

In this section, the influence of friction in the BS coupling is further analysed. All analyses are performed using the TR model with the radius difference $\Delta R = 15 \mu\text{m}$, which represents the sliding fit between the socket and the ball. The effect of various combinations of friction coefficients f_s and f_d is shown in Figs. 11, 12 and 13 for the Bengisu-Akay friction model, for the LuGre friction model with $\sigma_0^A = 10^6 \text{ m}^{-1}$ and for the LuGre friction model with $\sigma_0^A = 5 \cdot 10^6 \text{ m}^{-1}$, respectively. Figures show that with the increasing values of friction coefficients, the journal orbit is slightly larger. This fact confirms that the friction in the BS coupling negatively affects the rotor assembly. The journal orbits for both friction models are comparable in size and shape.

In the case of the Bengisu-Akay friction model, the regions of the sticking phenomenon with almost zero pad tilting velocity can be seen in the middle subfigure of Fig. 11. In these regions, the slope of the tilting velocity is not exactly zero because the friction model employs smoothing around the zero velocity, which is expressed by the critical velocity v_c as described earlier in Sect. 3.1. With the increase in friction coefficients, the sticking phenomenon areas are wider, and the amplitudes of the pad tilting velocities decrease. This deteriorates the dynamic behaviour of the whole TPJB.

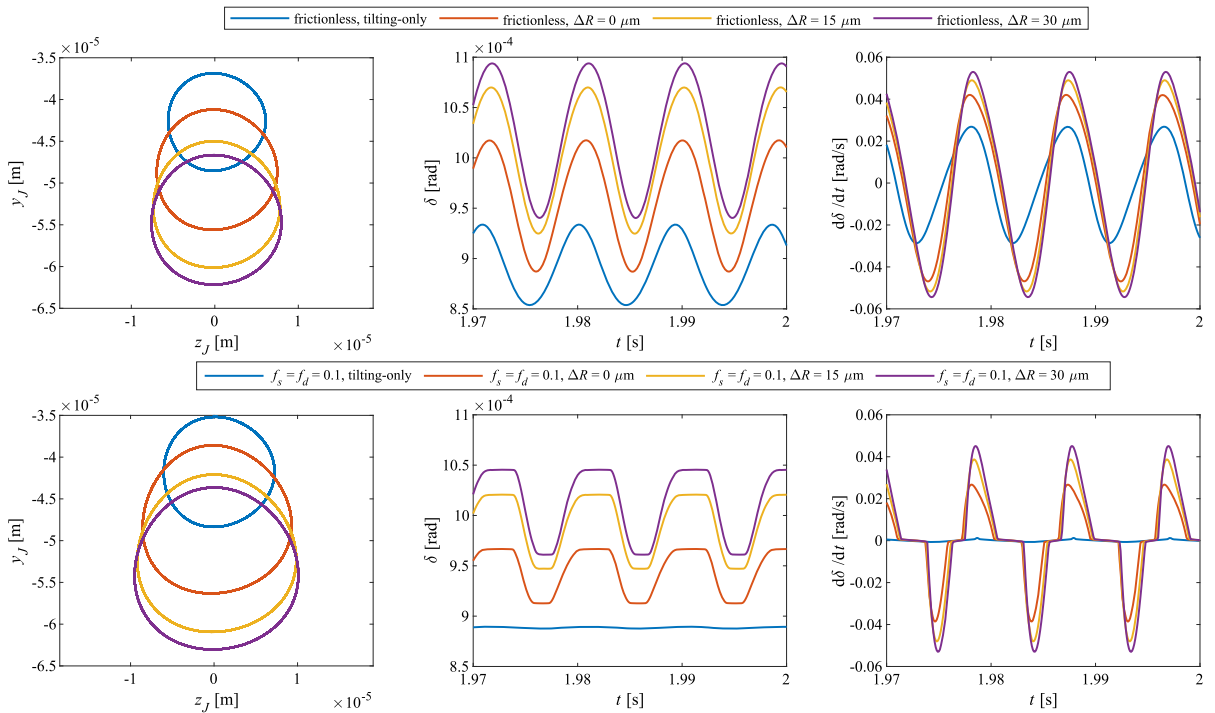


Fig. 10 Influence of the considered various radius differences on the journal orbit (left), tilting angle of pad (centre) and its tilting velocity (right). All the results are depicted for frictionless

(FL) case in the upper row) and a case with friction below (here, Bengisu-Akay model with $f = f_s = f_d = 0.1$ is used as an example). Tilting-only model is depicted for reference

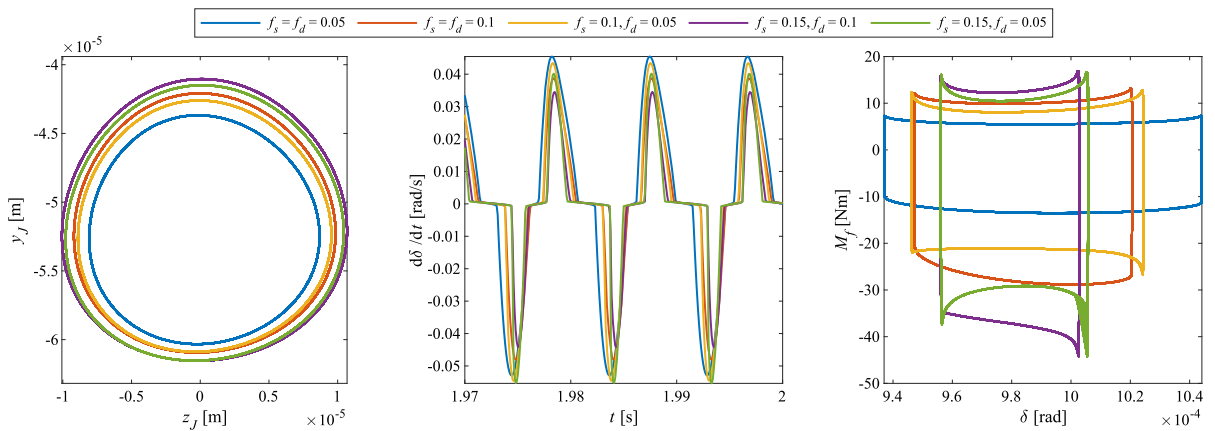


Fig. 11 The influence of various friction coefficients f_s and f_d of the Bengisu-Akay friction model on the journal orbit (left), pad tilting velocity (middle) and the resulting relation between frictional moment and pad tilting angle (right). Tilting-radial model with the same radius difference $\Delta R = 15 \mu\text{m}$ is assumed for all cases

tional moment and pad tilting angle (right). Tilting-radial model with the same radius difference $\Delta R = 15 \mu\text{m}$ is assumed for all cases

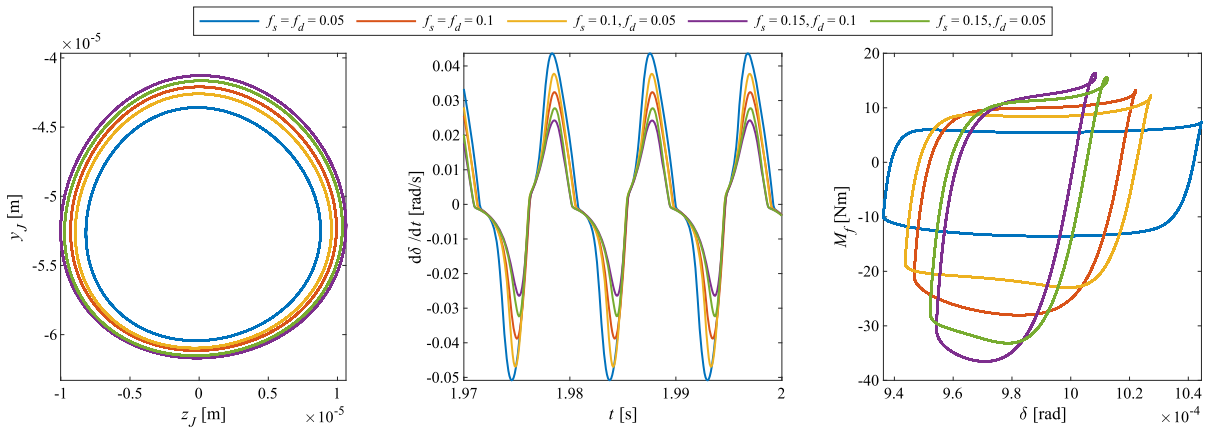


Fig. 12 The influence of various friction coefficients f_s and f_d of the LuGre friction model with $\sigma_0^A = 10^6 \text{ m}^{-1}$ on the journal orbit (left), pad tilting velocity (middle) and the resulting relation

between frictional moment and pad tilting angle (right). Tilting-radial model with the same radius difference $\Delta R = 15 \mu\text{m}$ is assumed for all cases

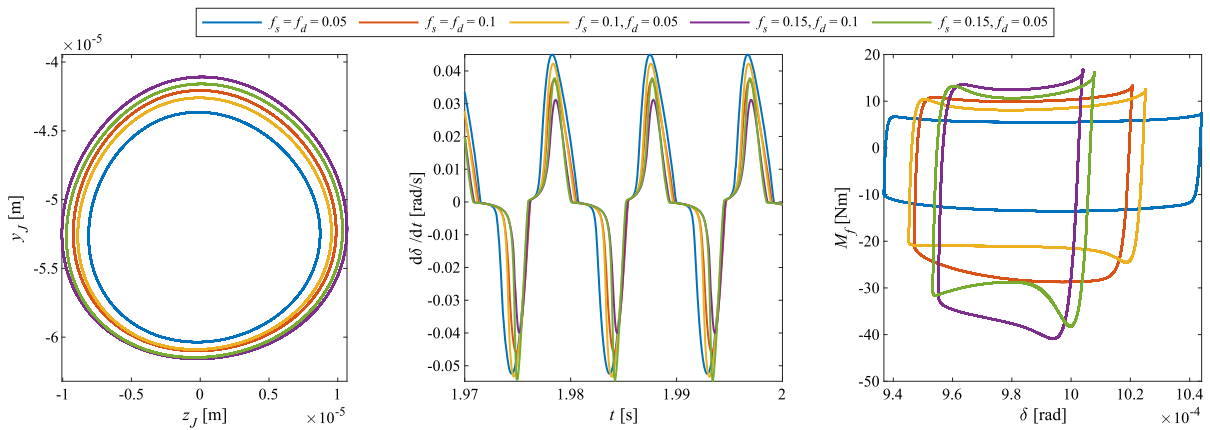


Fig. 13 The influence of various friction coefficients f_s and f_d of the LuGre friction model with $\sigma_0^A = 5 \cdot 10^6 \text{ m}^{-1}$ on the journal orbit (left), pad tilting velocity (middle) and the resulting relation

between frictional moment and pad tilting angle (right). Tilting-radial model with the same radius difference $\Delta R = 15 \mu\text{m}$ is assumed for all cases

For the LuGre friction model with $\sigma_0^A = 10^6 \text{ m}^{-1}$, the transition between the sticking and sliding is more smooth than for the Bengisu-Akay friction model, as seen on the pad tilting speed in the middle of Fig. 12. This is caused by the bristle stiffness and damping, which act similarly to a spring-damper in the sticking phase. With the increase in friction coefficients, the amplitude of the pad tilting velocity decreases more than in the case of the Bengisu-Akay friction model. This is also caused by the fact that, in the case of the LuGre model, the sticking phase is more elastic. Therefore, the pad tilts more smoothly during each cycle, so

it reaches lower velocities before its load due to the hydrodynamic force is minimum. In contrast, in the case of the Bengisu-Akay friction model, the pad moves more abruptly when the friction reaches its maximum static values.

The middle subfigure of Fig. 13 shows that with increased σ_0^A , the sticking phase is more distinct in the pad tilting velocity waveforms. The bristle are stiffer, thus smaller bristle deflection occurs before the maximum static friction force is reached and sliding occurs. With a further increase of σ_0^A , the resulting pad tilt-

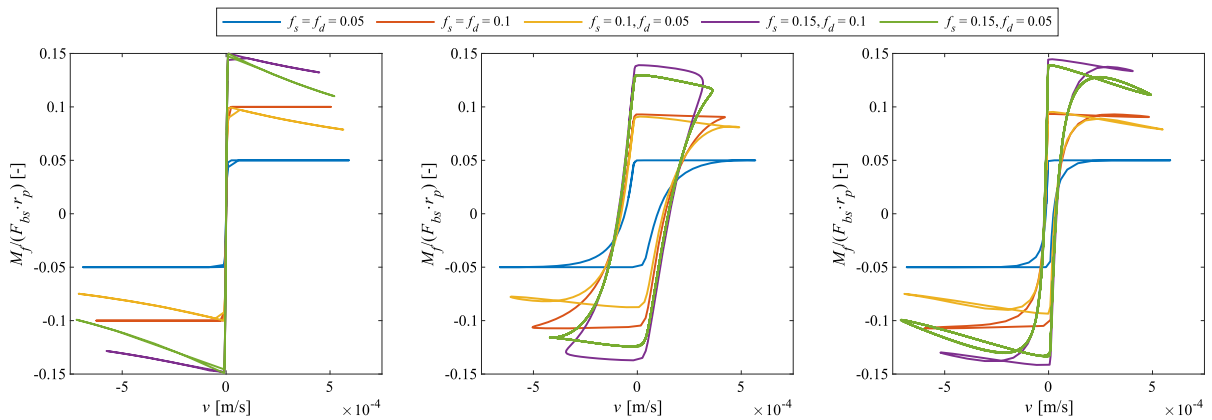


Fig. 14 The resulting friction characteristics when the Bengisu-Akay friction model (left), the LuGre friction model with $\sigma_0^A = 10^6 \text{ m}^{-1}$ (middle) and the LuGre friction model with $\sigma_0^A = 5 \cdot 10^6 \text{ m}^{-1}$ (right) is used

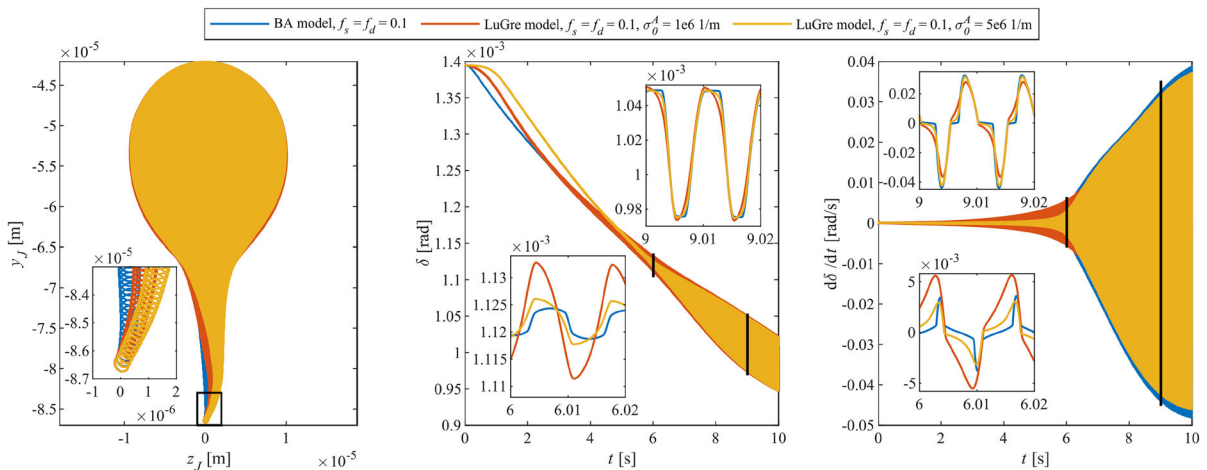


Fig. 15 Comparison of the Bengisu-Akay friction model and the LuGre friction model during run-up 1500 rpm to 6500 rpm – journal run-up trajectory (left) and corresponding waveform of tilting angle (centre) and velocity (right)

ing velocity curve shape is getting closer to the results obtained using the Bengisu-Akay model.

The right subfigure of Figs. 11, 12 and 13 shows the hysteresis loop (relation between the frictional moment and pad tilting angle) of the Bengisu-Akay friction model, the LuGre friction model with $\sigma_0^A = 10^6 \text{ m}^{-1}$ and the LuGre friction model with $\sigma_0^A = 5 \cdot 10^6 \text{ m}^{-1}$, respectively. It should be noted that the frictional moment depends on the normal radial force $F_{bs,i}$ that varies with the journal rotation, which affects the loop shape. However, in the case of the LuGre model, the loop has a more typical shape. In the case of the Bengisu-Akay model and the LuGre model with $\sigma_0^A = 5 \cdot 10^6 \text{ m}^{-1}$, the effect of different

values of f_s and f_d parameters is more significant and manifested by the convex and concave bending of the curve in the upper and lower parts, respectively.

In Fig. 14, the resulting relationship between the applied friction coefficient and the relative velocity in the BS coupling is shown. In this case, the applied friction coefficient is calculated as $M_f / (F_{bs} \cdot r_p)$ to eliminate the influence of the varying radial force $F_{bs,i}$ load of the BS. The resulting curve exactly corresponds to the used Stribeck curve in the case of the Bengisu-Akay model, while in the case of the LuGre model, the hysteresis behaviour is present. The typical friction curve loops appear in the case of a higher σ_0^A , while with the lower σ_0^A this phenomenon is not significant.

4.4 Influence of friction during run-up

The Bengisu-Akay and LuGre friction models analysed previously for various parameters σ_0^A were also examined during the run-up of the unbalanced rotor. In this case, the radius difference was considered as 15 μm . The run-up simulations for both friction models were performed in the speed range 1500 – 6500 rpm lasting 10 s. The results are summarised in Fig. 15. There is an apparent deviation in the journal trajectory for the LuGre model compared to the Bengisu-Akay model at lower rotor speed. A higher parameter value σ_0^A strengthens the deviation of the journal trajectory. The changes are depicted in detail for clarity. However, the journal orbits at 6500 rpm are comparable. Depicted details for tilting angle and velocity show that the results for $\sigma_0^A = 1 \cdot 10^6 \text{ m}^{-1}$ are different from the Bengisu-Akay model and higher σ_0^A at lower rotor speed. The influence of considered friction models and the parameter settings on tilting angle and velocity is not affected greatly by the run-up operation, and obtained results, e.g. sticking phase, correspond to the previous discussion for steady-state operations.

5 Conclusion

This work has provided an in-depth analysis of local phenomena occurring in pivots of tilting pad journal bearings (TPJB). In particular, we focused on modelling nonlinear normal force and friction forces generated in ball-and-socket couplings, which are used to support tilting pads. For the detailed model of friction forces, we used the Bengisu-Akay [19] and LuGre [21] friction models assuming a conformal sphere-to-sphere contact. The latter model captures such effects as stick-slip, presliding or breakaway force.

In agreement with previous research [6,7,9], friction plays an important negative role in the bearing performance. The friction causes resistance to the tilting motion, which decreases the bearing capability to accommodate the operating conditions. Consequently, friction in the pivots enlarges the vibration of the supported journal.

Friction also significantly affects the radial dynamic stiffness of the pivots. Low pivot stiffness can decrease the bearing performance under high radial loads. In such circumstances, the pivot can be compressed excessively, which enlarges the bearing operating clear-

ance. This phenomenon is critical when designating machining tolerances of the pivot. Too loose machining tolerances may lead to a too-high radius difference. Although the bearing can be assembled so that the radius difference does not influence its clearance, the radius difference decreases the dynamic stiffness considerably. Thus, the radial load can compress the pivot more than expected, increasing the bearing clearance. Concerning this fact, correctly estimating the force-deformation dependence in the ball-and-socket coupling is essential.

The results indicate that unbalance excitation is also essential for the TPJB dynamics. The additional forcing due to unbalance affects the stick and slip regimes and can enforce sticking at lower operating speeds (and thus eliminates the slip).

A broad discussion has been dedicated to the correct choice of friction parameters. It has been shown that the generic and usually used values of some parameters, such as critical velocity v_s , would give misleading results. Therefore, they should be chosen carefully with respect to the problem being solved. Furthermore, concerning the LuGre friction model, it is also necessary to use an “amended” model which adopts the friction model for the case with a time-varying normal load.

Figs. 11, 12 and 13 show that increasing the σ_0^A parameter of the LuGre friction model brings the results closer to the Bengisu-Akay friction model under steady-state conditions. However, increasing the σ_0^A parameter still does not guarantee that the results of transient simulations will be equal, as shown in Fig. 15. This finding strengthens the fact that simple static models do not include various frictional effects, which can non-negligibly affect the TPJB dynamics.

The work demonstrates that precise BS friction modelling can play an essential role in the computational modelling of whole rotor systems. The detailed models allow a more profound analysis of various rotor nonlinear phenomena, such as fretting wear in contact areas, pivot durability and clearance analysis. The sticking and sliding regimes can also influence undesirable behaviour in TPJBs with lightly loaded pads, including pad fluttering and spragging [22].

Detailed modelling of undesirable phenomena present in the TPJBs during their operation improves the knowledge about the TPJB performance. It can decrease the financial costs due to extending regular maintenance intervals and necessary parts replacement. In the future, the proposed approach can be used as a

base for modelling conformal ball-and-socket pivots involving friction.

Acknowledgements This paper was supported by the Technology Agency of the Czech Republic under the THETA Programme within the TK04020057 project.

Author contributions S.D. involved in conceptualisation, formal analysis, methodology, software, validation, visualisation, writing original draft. J.R. involved in conceptualisation, formal analysis, methodology, software, validation, visualisation, writing original draft. R.B. involved in conceptualisation, formal analysis, methodology, software, validation, visualisation, writing original draft. L.S. involved in formal analysis, funding acquisition, project administration, supervision, validation, writing original draft.

Funding Open access publishing supported by the National Technical Library in Prague. The authors have not disclosed any funding.

Data availability The datasets generated during and/or analysed during the current study are available from the corresponding author on reasonable request.

Declarations

Conflicts of interest The authors declare that they have no conflict of interest.

Open Access This article is licensed under a Creative Commons Attribution 4.0 International License, which permits use, sharing, adaptation, distribution and reproduction in any medium or format, as long as you give appropriate credit to the original author(s) and the source, provide a link to the Creative Commons licence, and indicate if changes were made. The images or other third party material in this article are included in the article's Creative Commons licence, unless indicated otherwise in a credit line to the material. If material is not included in the article's Creative Commons licence and your intended use is not permitted by statutory regulation or exceeds the permitted use, you will need to obtain permission directly from the copyright holder. To view a copy of this licence, visit <http://creativecommons.org/licenses/by/4.0/>.

References

- Nicholas, J., Wygant, K.: Tilting Pad Journal Bearing Pivot Design for High Load Applications. In: Proceedings of the 24th Turbomachinery Symposium, Turbomachinery Laboratory, Texas A&M University, 1995, pp. 33–47
- Wygant, K.D., Flack, R.D., Barrett, L.E.: Measured performance of tilting-pad journal bearings over a range of preloads-part I: static operating conditions. *Tribol. Trans.* **47**(4), 576–584 (2004). <https://doi.org/10.1080/05698190490504154>
- Wygant, K.D., Barrett, L.E., Flack, R.D.: Influence of pad pivot friction on tilting-pad journal bearing measurements-part II: dynamic coefficient. *Tribol. Trans.* **42**(1), 250–256 (1999). <https://doi.org/10.1080/10402009908982215>
- Pettinato, B., Choudhury, P.D.: Test results of key and spherical pivot five-shoe tilt pad journal bearings-part I: performance measurements. *Tribol. Trans.* **42**(3), 541–547 (1999). <https://doi.org/10.1080/10402009908982253>
- Pettinato, B., Choudhury, P.D.: Test results of key and spherical pivot five-shoe tilt pad journal bearings-part II: dynamic measurements. *Tribol. Trans.* **42**(3), 675–680 (1999). <https://doi.org/10.1080/10402009908982269>
- Kim, S.-G., Kim, K.-W.: Influence of pad-pivot friction on tilting pad journal bearing. *Tribol. Int.* **41**(8), 694–703 (2008). <https://doi.org/10.1016/j.triboint.2007.12.003>. <https://www.sciencedirect.com/science/article/pii/S0301679X07002113>
- F. He, Including pivot friction in pad motion for a tilting pad journal bearing with ball-socket pivots, Vol. Volume 7A: Structures and Dynamics of Turbo Expo: Power for Land, Sea, and Air, 2017, pp. 1–11, v07AT34A036. <https://doi.org/10.1115/GT2017-65240>. <https://asmedigitalcollection.asme.org/GT/proceedings-pdf/GT2017/50923/V07AT34A036/2434503/v07at34a036-gt2017-65240.pdf>
- Kim, S., Byun, S., Suh, J.: Effects of tilting pad journal bearing design parameters on the pad-pivot friction and nonlinear rotordynamic bifurcations, *Appl. Sci.* **10** (16). <https://doi.org/10.3390/app10165406>. <https://www.mdpi.com/2076-3417/10/16/5406>
- Kim, S., Palazzolo, A. B.: Pad-pivot friction effect on nonlinear response of a rotor supported by tilting-pad journal bearings, *J. Tribol.* **141** (9), 091701. <https://doi.org/10.1115/1.4043971>. https://asmedigitalcollection.asme.org/tribology/article-pdf/141/9/091701/6420906/trib_141_9_091701.pdf
- Shin, D., Palazzolo, A. B.: Tilting pad bearing pivot friction and design effects on thermal bow-induced rotor vibration, *J. Tribol.* **143** (12), 121804. <https://doi.org/10.1115/1.4050427>. https://asmedigitalcollection.asme.org/tribology/article-pdf/143/12/121804/6672322/trib_143_12_121804.pdf
- Gu, L.: A review of Morton effect: from theory to industrial practice. *Tribol. Trans.* **61**(2), 381–391 (2018). <https://doi.org/10.1080/10402004.2017.1333663>
- Dang, P. V., Chatterton, S., Pennacchi, P.: The effect of the pivot stiffness on the performances of five-pad tilting pad bearings, *Lubricants* **7** (7). <https://doi.org/10.3390/lubricants7070061>. <https://www.mdpi.com/2075-4442/7/7/61>
- Ciulli, E., Forte, P., Antonelli, F., Minelli, R., Panara, D.: Tilting pad journal bearing ball and socket pivots: experimental determination of stiffness, *Machines* **10** (2). <https://doi.org/10.3390/machines10020081>. <https://www.mdpi.com/2075-1702/10/2/81>
- Kirk, R.G., Reedy, S.W.: Evaluation of pivot stiffness for typical tilting-pad journal bearing designs. *J. Vibration Acoustics Stress Reliabil. Des.* **110**(2), 165–171 (1988). <https://doi.org/10.1115/1.3269494>. https://asmedigitalcollection.asme.org/vibrationacoustics/article-pdf/110/2/165/5434996/165_1.pdf

15. Shi, Z., Jin, Y., Yuan, X.: Influence of pivot design on nonlinear dynamic analysis of vertical and horizontal rotors in tilting pad journal bearings. *Tribol. Int.* **140**, 105859 (2019). <https://doi.org/10.1016/j.triboint.2019.105859>.<https://www.sciencedirect.com/science/article/pii/S0301679X19303664>
16. Fang, X., Zhang, C., Chen, X., Wang, Y., Tan, Y.: A new universal approximate model for conformal contact and non-conformal contact of spherical surfaces. *Acta Mechanica* **226**, 1657–1672 (2015). <https://doi.org/10.1007/s00707-014-1277-z>
17. Kubenko, V., Yanchevskiy, I.V.: Axisymmetric nonstationary elastic contact problem for conforming surfaces. *Archive Appl. Mech.* **88**(9), 1559–1571 (2018). <https://doi.org/10.1007/s00419-018-1387-5>
18. Ciavarella, M.: A JKR solution for a ball-in-socket contact geometry as a bi-stable adhesive system. *Acta Mech.* **229**(7), 2835–2842 (2018). <https://doi.org/10.1007/s00707-018-2138-y>
19. Marques, F., Flores, P., Pimenta Claro, J.C., Lankarani, H.M.: A survey and comparison of several friction force models for dynamic analysis of multibody mechanical systems. *Nonlinear Dyn.* **86**(3), 1407–1443 (2016). <https://doi.org/10.1007/s11071-016-2999-3>
20. Bengisu, M., Akay, A.: Stability of friction-induced vibrations in multi-degree-of-freedom systems. *J. Sound Vibration* **171**(4), 557–570 (1994). <https://doi.org/10.1006/jsvi.1994.1140>.<https://www.sciencedirect.com/science/article/pii/S0022460X84711400>
21. Canudas de Wit, C., Olsson, H., Astrom, K., Lischinsky, P.: A new model for control of systems with friction. *IEEE Trans. Automat. Control* **40**(3), 419–425 (1995). <https://doi.org/10.1109/9.376053>
22. Rendl, J., Dyk, Š., Smolík, L.: Nonlinear dynamic analysis of a tilting pad journal bearing subjected to pad fluttering. *Nonlinear Dyn.* **105**(3), 2133–2156 (2021). <https://doi.org/10.1007/s11071-021-06748-x>
23. Mehdi, S.M., Jang, K.E., Kim, T.H.: Effects of pivot design on performance of tilting pad journal bearings. *Tribol. Int.* **119**, 175–189 (2018). <https://doi.org/10.1016/j.triboint.2017.08.025>.<https://www.sciencedirect.com/science/article/pii/S0301679X17304140>
24. Canudas de Wit, C., Tsiotras, P.: Dynamic Tire Friction Models for Vehicle Traction Control. In: Proceedings of the 38th IEEE Conference on Decision and Control (Cat. No.99CH36304), Vol. 4, 1999, pp. 3746–3751 vol.4. <https://doi.org/10.1109/CDC.1999.827937>
25. Marques, F., Woliński, L., Wojtyra, M., Flores, P., Lankarani, H.M.: An investigation of a novel LuGre-based friction force model. *Mech. Machine Theory* **166**, 104493 (2021). <https://doi.org/10.1016/j.mechmachtheory.2021.104493>.<https://www.sciencedirect.com/science/article/pii/S0094114X21002500>
26. Colantonio, L., Dehombreux, P., Hajžman, M., Verlinden, O.: 3D projection of the LuGre friction model adapted to varying normal forces. *Multibody Syst. Dyn.* (2022). <https://doi.org/10.1007/s11044-022-09820-5>
27. Sun, Y.-H., Chen, T., Wu, C.Q., Shafai, C.: A comprehensive experimental setup for identification of friction model parameters. *Mech. Machine Theory* **100**, 338–357 (2016). <https://doi.org/10.1016/j.mechmachtheory.2016.02.013>.<https://www.sciencedirect.com/science/article/pii/S0094114X16000501>
28. Haugaard, A.M., Santos, I.F.: Stability of multi orifice active tilting-pad journal bearings. *Tribol. Int.* **43**(9), 1742–1750 (2010). <https://doi.org/10.1016/j.triboint.2010.04.013>.<http://www.sciencedirect.com/science/article/pii/S0301679X10001106>
29. ISO 21940-11: Mechanical vibration – rotor balancing – part 11: Procedures and tolerances for rotors with rigid behaviour, Standard, International Organization for Standardization, Geneva (2016)
30. Piatkowski, T.: Dahl and LuGre dynamic friction models - the analysis of selected properties. *Mech. Machine Theory* **73**, 91–100 (2014). <https://doi.org/10.1016/j.mechmachtheory.2013.10.009>.<https://www.sciencedirect.com/science/article/pii/S0094114X13002152>
31. Deur, J., Asgari, J., Hrovat, D.: A 3D brush-type dynamic tire friction model. *Vehicle Syst. Dyn.* **42**(3), 133–173 (2004). <https://doi.org/10.1080/00423110412331282887>
32. Zhou, Z., Zheng, X., Wang, Q., Chen, Z., Sun, Y., Liang, B.: Modeling and simulation of point contact multibody system dynamics based on the 2d LuGre friction model. *Mech. Machine Theory* **158**, 104244 (2021). <https://doi.org/10.1016/j.mechmachtheory.2021.104244>.<https://www.sciencedirect.com/science/article/pii/S0094114X21000021>
33. ISO 286-1: Geometrical product specifications (GPS) – ISO code system for tolerances on linear sizes – part 1: Basis of tolerances, deviations and fits, Standard, International Organization for Standardization, Geneva (2010)

Publisher's Note Springer Nature remains neutral with regard to jurisdictional claims in published maps and institutional affiliations.